SCIENCE CHINA
Information Sciences

• RESEARCH PAPER •

August 2022, Vol. 65 182302:1–182302:15
https://doi.org/10.1007/s11432-021-3343-7

Time and energy efficient data collection via UAV

Tianhao WANG[1], Xiaowei PANG[1], Jie TANG[2], Nan ZHAO[1*], Xiuyin ZHANG[2] & Xianbin WANG[3]

[1]*School of Information and Communication Engineering, Dalian University of Technology, Dalian* 116024*, China;*
[2]*School of Electronic and Information Engineering, South China University of Technology, Guangzhou* 510641*, China;*
[3]*Department of Electrical and Computer Engineering, Western University, London* ON N6A 5B9*, Canada*

Received 3 June 2021/Revised 30 August 2021/Accepted 8 October 2021/Published online 25 July 2022

Abstract Using unmanned aerial vehicles (UAVs) for data collection has emerged as a promising technique to achieve both time- and energy-efficient data gathering while keeping data fresh. In this study, two schemes are proposed for flight cycle minimization and energy efficiency maximization to collect data from ground sensors. We first minimize the flight cycle by jointly optimizing the wake-up scheduling of sensors, the trajectory, and the time slot, which is a mixed-integer non-convex problem and difficult to solve directly. To this end, we propose an iterative algorithm based on block coordinate descent and successive convex approximation to decouple the original non-convex problem into two sub-problems and the constraints are turned to be convex approximately. Furthermore, the energy efficiency is maximized since the limited energy is a critical issue in UAV communication systems. We approximate the two subproblems as convex optimizations by introducing slack variables and applying SCA. The approximate energy efficiency is a fractional expression, and we use Dinkelbach's method to solve it. Numerical results show that the flight cycle is minimized in the first scheme with the data requirement satisfied, while in the second scheme, the energy efficiency is maximized with the trade-off between the transmission data and the propulsion power consumption.

Keywords data collection, energy efficiency maximization, time minimization, trajectory optimization, unmanned aerial vehicle (UAV)

Citation Wang T H, Pang X W, Tang J, et al. Time and energy efficient data collection via UAV. Sci China Inf Sci, 2022, 65(8): 182302, https://doi.org/10.1007/s11432-021-3343-7

1 Introduction

Unmanned aerial vehicles (UAVs) have attracted extensive attention due to their high mobility, swift deployment, and low cost [1–3]. As a low-altitude platform, UAV may establish better wireless channels with ground nodes due to line-of-sight (LoS) links, which can significantly enhance the system throughput and save the transmit power [4]. In particular, UAVs can be deployed in various applications such as seamless coverage [5], aerial base stations (BSs) [6], mobile relaying [7], and cellular data offloading [8]. Especially, there is increasing research effort on data collection enabled by UAVs due to their flexibility and reliability.

For data collection purpose, UAVs can be deployed with inherent wireless sensor networks (WSNs) where the sensing data are collected from ground terminals in [9–11], which have found many applications, such as precision agriculture, weather monitoring, and distributed estimation. Compared with the conventional ground sensor networks, exploiting UAV as a flying data collector can gather sensing data from distributed sensors efficiently and reliably, and each sensor node can transmit data in a much better air-ground channel while guaranteeing fairness among users. An energy-efficient design in UAV-aided WSN is proposed by Zhan et al. [12] to minimize the maximum energy consumption of all sensors. They also investigate a multi-UAV enabled WSN to study the fundamental tradeoff between aerial energy cost and ground energy cost in [13]. Therefore, UAV-aided data collection can enhance performance and improve the lifetime of WSNs.

* Corresponding author (email: zhaonan@dlut.edu.cn)

Despite the wide utilization of UAVs, one critical issue is the limited endurance, which greatly restricts the lifetime of UAVs and limits their applications [14–16]. Furthermore, it is also important to reduce the flight cycle for a given task so that the subsequent missions can start as soon as possible. Thus, time-efficient communication for minimizing the flight time is of paramount importance [17–20]. Zeng et al. [17] minimized the mission time while ensuring high success probability of file recovery. Zhan et al. [18] considered a general multi-UAV enabled WSN and proposed two schemes of hovering mode and flying mode, aiming to minimize the maximum mission time among all UAVs. Gong et al. [19] considered a scenario where a set of energy-constrained sensors are placed along a line and studied the flight time minimization problem with the data upload requirement. They further studied a general scenario where sensors are randomly located on a two-dimensional (2D) ground space [20].

On the other hand, it is worthwhile to mention that the minimum flight cycle does not mean the minimum UAV's energy consumption due to the complex factors, i.e., the UAV energy consumption also lies in flying, hovering and other operations [21–23]. In [23], the UAV energy consumption was simulated according to flight speed and operating conditions such as lifting and hovering. Zeng et al. [24] studied the energy minimization problem of rotary-wing UAV and derived a rigorous energy consumption model which can be applied in cellular network [25], wireless power transfer [26], and many other scenarios. For this challenging non-convex problem, it applies successive convex approximation (SCA) to solve it. The optimal transmission scheduling was proposed by Li et al [27]. To minimize the maximum UAV energy consumption with the guarantee of bit error rate. Hua et al. [28] minimized the UAV power consumption while satisfying the rate requirements of sensors. In fact, we prefer to study the energy-efficient communication for collecting more data per unit of UAV's energy consumption due to the limited on-board energy. Zeng et al. [29] derived the propulsion energy consumption of fixed-wing UAVs as a function of flying velocity and acceleration and studied the energy efficiency maximization problem subject to the general constraints of UAVs and sensors. The design of energy-efficient communication in a UAV-assisted backscatter communication network was proposed by Yang et al. [30] to maximize the energy efficiency of the network. Pang et al. [31] investigated the maximum energy efficiency of the mmWave-enabled NOMA-UAV networks via optimizing the UAV placement, hybrid precoding, and power allocation.

Motivated by the above-mentioned studies, we investigate the data collection of limited-energy UAVs from two aspects, time efficiency and energy efficiency. For time-efficient data collection, minimizing the flight cycle can keep sensing data fresh and allow subsequent missions to start early. For energy-efficient data collection, maximizing the energy efficiency ensures that the UAV collects more data with limited energy. We consider a general scenario where a UAV is deployed to serve some energy-constrained ground sensors. The main contributions of this paper are summarized as follows:

• First, we consider a general UAV-enabled WSN, where a rotary-wing UAV is dispatched to collect data periodically from ground sensors with limited energy. Two optimization problems are formulated to minimize the flight cycle and maximize the energy efficiency, via jointly optimizing the wake-up scheduling of sensors, the UAV trajectory, and the time slot. Both the two problems are mixed-integer non-convex problems with coupled variables, which are difficult to solve directly.

• To tackle the flight cycle minimization problem, a general iterative algorithm using block coordinate descent (BCD) [32] and SCA [33] is proposed. Specifically, we use BCD to transform the original problem into two subproblems: the wake-up scheduling optimization with fixed trajectory and the trajectory optimization with fixed wake-up scheduling. The two non-convex subproblems are approximated as convex by SCA. The convergence and complexity of the proposed algorithm are also analyzed.

• For the energy efficiency maximization problem, we propose an algorithm based on BCD and SCA. Two transformed subproblems are formulated: the wake-up scheduling and time slot optimization, as well as the trajectory optimization. We transform the two subproblems into approximate convex optimizations by introducing slack variables and employing SCA. Since the approximate optimization objective is a fractional expression of trajectory, wake-up scheduling, and time slot, we use the Dinkelbach's method [34] to tackle the fractional programming (FP) problem and gain a suboptimal solution.

The rest of this paper is organized as follows. In Section 2, we introduce the system model and problem formulation. Section 3 studies the flight cycle minimization optimization problem based on BCD and SCA. Section 4 studies the energy efficiency maximization optimization problem via the Dinkelbach's method. In Section 5, we present the simulation results to illustrate the proposed algorithms, followed by the conclusion in Section 6.

Notation. In this paper, matrix, vector, and scalar are denoted by bold uppercase letter $\boldsymbol{A}$, bold

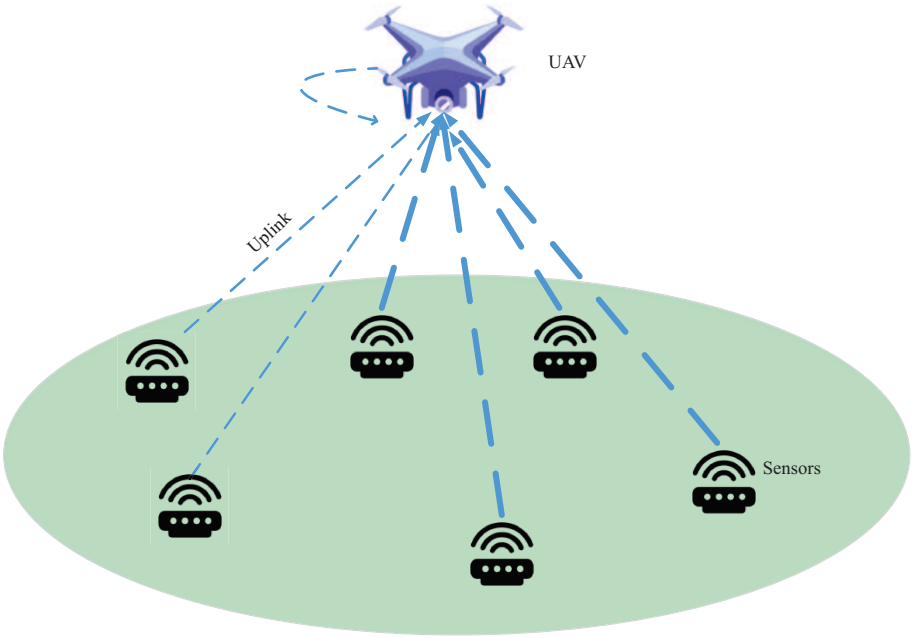

Figure 1 (Color online) UAV-aided data collection in wireless sensor networks.

lowercase letter $\boldsymbol{a}$, and lowercase letter a. $\|\boldsymbol{A}\|$ and $\|\boldsymbol{a}\|$ denote the Frobenius norm and the Euclidean norm, respectively. $\boldsymbol{A}^{\mathrm{T}}$ represents the transpose of $\boldsymbol{A}$. $\mathbb{R}^{x\times y}$ denotes the space of $x \times y$ real matrices. Finally, $\triangleq$ means equivalence in definition.

2 System model

As shown in Figure 1, we consider the uplink communication in a UAV-aided WSN, where a UAV collects data from ground sensors via time-division multiple access. The UAV flies at a fixed altitude H with a maximum speed V_m and a flight cycle T. Denote the set of ground sensors as $\mathcal{I} \triangleq \{1, 2, \ldots, I\}$. The ith sensor is located at $\boldsymbol{L}_i = [x_i, y_i]^{\mathrm{T}} \in \mathbb{R}^{2\times 1}$, and transmits at least B_i to the UAV in each cycle with an energy budget of E_i, $\forall i \in \mathcal{I}$. We divide the flight cycle T into N time slots, with the duration of each time slot $\delta_t = T/N$. Let $\mathcal{N} \triangleq \{1, 2, \ldots, N\}$ denote the set of time slots. The number of time slots N should be large enough to ensure that the location of the UAV is approximately unchanged.

Denote the 2D Cartesian coordinate of UAV in the nth time slot as $\boldsymbol{w}[n] = [x[n], y[n]]^{\mathrm{T}}$, $n = 1, 2, \ldots, N$, and the initial and final locations of a UAV are $\boldsymbol{w}[1]$ and $\boldsymbol{w}[N]$, respectively. The UAV returns to its initial location at the end of each flight cycle, and the maximum speed is denoted as V_m. As a result, we have

$$\boldsymbol{w}[1] = \boldsymbol{w}[N], \tag{1}$$

$$\|\boldsymbol{w}[n+1] - \boldsymbol{w}[n]\| \leqslant V_m \delta_t, \quad n = 1, \ldots, N-1, \tag{2}$$

$$\|\boldsymbol{w}[n+1] - \boldsymbol{w}[n]\|^2 \leqslant \gamma H^2, \quad n = 1, \ldots, N-1, \tag{3}$$

where γ should be carefully chosen to guarantee that the UAV's location is approximately unchanged within each time slot.

Assume that the UAV only serves at most one sensor in each time slot. Define a binary variable $S_i[n]$ to illustrate the wake-up scheduling of sensors, which implies that the UAV serves the ith sensor in time slot n if $S_i[n] = 1$, while $S_i[n] = 0$ means that the ith sensor is not served by the UAV in the nth time slot. Therefore, the wake-up scheduling of sensors should satisfy

$$S_i[n] = \{0, 1\}, \ \forall i \in \mathcal{I}, \ \forall n \in \mathcal{N}, \tag{4}$$

$$\sum_{i\in\mathcal{I}} S_i[n] \leqslant 1, \ \forall n \in \mathcal{N}. \tag{5}$$

Generally, the UAV-ground channel needs to consider both the LoS and non-LoS (NLoS) [35–37]. According to [38], the LoS probability can be approximated to 1 when the UAV is above 100 m, which is suitable for the proposed scheme. Thus it can be assumed that the UAV-ground channels in this study are dominated by LoS, which has been also adopted in existing literatures [29–31, 39, 40]. The distance between the UAV and the ith sensor in the nth time slot can be expressed as

$$d^i[n] = \sqrt{H^2 + \|\boldsymbol{w}[n] - \boldsymbol{L}_i\|^2},\ \forall i \in \mathcal{I}. \tag{6}$$

Therefore, the channel power gain from the ith sensor to the UAV can be modeled as

$$h^i[n] = \frac{\rho_0}{H^2 + \|\boldsymbol{w}[n] - \boldsymbol{L}_i\|^2},\ \forall i \in \mathcal{I}, \tag{7}$$

where ρ_0 denotes the reference channel power gain at the distance $d_0 = 1$ m. Thus, the achievable transmission rate for the ith sensor in the nth time slot can be expressed as

$$R_u^i[n] = S_i[n]\log_2\left(1 + \frac{P_A\rho_0}{(H^2 + \|\boldsymbol{w}[n] - \boldsymbol{L}_i\|^2)\sigma^2}\right), \tag{8}$$

where σ^2 is the additive Gauss white noise at the UAV, and P_A is the uplink transmit power of each sensor. For the ith sensor, it needs to transmit B_i within N time slots with the energy constraint E_i, which should satisfy

$$\sum_{n=1}^{N}(R_u^i[n]\delta_t) \geqslant B_i,\ \forall i \in \mathcal{I}, \tag{9}$$

$$\sum_{n=1}^{N}(S_i[n]P_A\delta_t) \leqslant E_i,\ \forall i \in \mathcal{I}. \tag{10}$$

For UAV-aided data collection, data freshness is a critical criterion. In addition, the finite on-board energy of a UAV limits its endurance and performance. Therefore, in the following sections, the flight cycle and energy efficiency are optimized for the data collection in UAV-aided WSNs, respectively.

3 Time-efficient data collection via UAV

In UAV-aided WSNs, time-efficient data collection is appealing for both UAVs and sensors to ensure the freshness of data. Thus we first propose a time-efficient data collection scheme in this section.

3.1 Problem formulation

We aim at minimizing the UAV flight cycle via jointly optimizing the wake-up scheduling of sensors $\boldsymbol{S} = \{S_i[n], \forall i \in \mathcal{I}, \forall n\}$, UAV trajectory $\boldsymbol{W} = \{\boldsymbol{w}[n], \forall n\}$ and the duration δ_t of each time slot with the aforementioned constraints. Notice that N is fixed, and we turn to find the minimum δ_t. The optimization problem can be formulated as

$$\min_{\boldsymbol{S},\boldsymbol{W},\delta_t}\ \delta_t \tag{11a}$$

$$\text{s.t. } (1), (2), (3), (4), (5), (9), (10), \tag{11b}$$

which is mathematically intractable as it is a mixed-integer non-convex problem. To solve it effectively, we set $\hat{t} = 1/\delta_t$, and relax the binary variables $S_i[n]$ into continuous variables. The problem (11) can be reformulated as

$$\max_{\boldsymbol{S},\boldsymbol{W},\hat{t}}\ \hat{t} \tag{12a}$$

$$\text{s.t. } \hat{t} \leqslant \frac{V_m}{\|\boldsymbol{w}[n+1] - \boldsymbol{w}[n]\|},\ n = 1, \ldots, N-1, \tag{12b}$$

$$0 \leqslant S_i[n] \leqslant 1,\ \forall i \in \mathcal{I},\ \forall n \in \mathcal{N}, \tag{12c}$$

$$\hat{t} \leqslant \frac{1}{B_i} \sum_{n=1}^{N} R_u^i[n],\ \forall i \in \mathcal{I}, \tag{12d}$$

$$\hat{t} \geqslant \frac{1}{E_i} \sum_{n=1}^{N} (S_i[n] P_A),\ \forall i \in \mathcal{I}, \tag{12e}$$

$$(1), (3), (5). \tag{12f}$$

Although relaxed, Eq. (12) is still difficult to solve because of the non-convex (12b) and (12d). In the following subsections, we use BCD to split it into two subproblems and exploit SCA to handle them.

3.2 Subproblem 1: wake-up scheduling optimization

For any given UAV trajectory $\boldsymbol{W}$, the wake-up scheduling optimization in (12) can be transformed as

$$\max_{\boldsymbol{S}, \hat{t}}\ \hat{t} \tag{13a}$$

$$\text{s.t. } (5), (12b), (12c), (12d), (12e). \tag{13b}$$

Note that in (8), $R_u^i[n]$ is a linear function with respect to $S_i[n]$. Thus, Eq. (13) is a standard linear programming problem, which can be solved by optimization tools such as CVX.

3.3 Subproblem 2: UAV trajectory optimization

With fixed wake-up scheduling $\boldsymbol{S}$, the UAV trajectory can be optimized by

$$\max_{\boldsymbol{W}, \hat{t}}\ \hat{t} \tag{14a}$$

$$\text{s.t. } (1), (3), (12b), (12d), (12e). \tag{14b}$$

Since Eqs. (12b) and (12d) are non-convex, it is difficult to solve it directly to obtain the optimal solution. Thus, we apply SCA to approximate the original function into a tractable one. Note that in the $(r+1)$th iteration, we first solve (13) and obtain solutions $\hat{t}_{\boldsymbol{S}}^{r+1}$ and $\boldsymbol{S}^{r+1}$. Then, for the constraint (12b), it is equivalent to

$$\|\boldsymbol{w}[n+1] - \boldsymbol{w}[n]\|^2 \leqslant \left(V_m/\hat{t}\right)^2,\ n = 1, \ldots, N-1, \tag{15}$$

which is non-convex with respect to $\hat{t}$. Apply the first-order Taylor expansion at the given point $\hat{t}_{\boldsymbol{S}}^{r+1}$ as

$$\left(\frac{V_m}{\hat{t}}\right)^2 \geqslant \left(\frac{V_m}{\hat{t}_{\boldsymbol{S}}^{r+1}}\right)^2 - \frac{2V_m^2}{\left(\hat{t}_{\boldsymbol{S}}^{r+1}\right)^3} \left(\hat{t} - \hat{t}_{\boldsymbol{S}}^{r+1}\right), \tag{16}$$

where $\hat{t}_{\boldsymbol{S}}^{r+1}$ is the optimal value of $\hat{t}$ for (13) calculated in the $(r+1)$th iteration. The right-hand side of (16) is a linear function of $\hat{t}$. Thus, the non-convex constraint (12b) can be approximated as

$$\|\boldsymbol{w}[n+1] - \boldsymbol{w}[n]\|^2 \leqslant \left(\frac{V_m}{\hat{t}_{\boldsymbol{S}}^{r+1}}\right)^2 - \frac{2V_m^2}{\left(\hat{t}_{\boldsymbol{S}}^{r+1}\right)^3} \left(\hat{t} - \hat{t}_{\boldsymbol{S}}^{r+1}\right). \tag{17}$$

For the constraint (12d), we introduce Proposition 1 to handle it.

Proposition 1. The non-convex constraint (12d) can be approximated as

$$\hat{t} \leqslant \frac{1}{B_i} \sum_{n=1}^{N} R_u^{i,lb}[n],\ \forall i \in \mathcal{I}, \tag{18}$$

where

$$R_u^{i,lb}[n] = A_i^r[n] + B_i^r[n] \left(\|\boldsymbol{w}[n] - \boldsymbol{L}_i\|^2 - \|\boldsymbol{w}^r[n] - \boldsymbol{L}_i\|^2\right). \tag{19}$$

In (19), $A_i^r[n]$ and $B_i^r[n]$ are constants defined as

$$A_i^r[n] = S_i[n]\log_2\left(1+\frac{P_A\rho_0}{(H^2+\|\boldsymbol{w}^r[n]-\boldsymbol{L}_i\|^2)\sigma^2}\right),\ \forall i,\ \forall n, \tag{20}$$

$$B_i^r[n] = -\frac{\frac{P_A\rho_0}{(H^2+\|\boldsymbol{w}^r[n]-\boldsymbol{L}_i\|^2)^2\sigma^2}}{1+\frac{P_A\rho_0}{(H^2+\|\boldsymbol{w}^r[n]-\boldsymbol{L}_i\|^2)\sigma^2}}\log_2 e,\ \forall i,\forall n. \tag{21}$$

Proof. Note that in the constraint (12d), $R_u^i[n]$ is neither convex nor concave with respect to $\boldsymbol{w}[n]$, but is convex with respect to $\|\boldsymbol{w}[n]-\boldsymbol{L}_i\|$. Thus, we replace $R_u^i[n]$ with its first-order Taylor expansion, and it can be lower-bounded as

$$R_u^i[n] \geqslant A_i^r[n]+B_i^r[n]\left(\|\boldsymbol{w}[n]-\boldsymbol{L}_i\|^2-\|\boldsymbol{w}^r[n]-\boldsymbol{L}_i\|^2\right) \triangleq R_u^{i,lb}[n], \tag{22}$$

where $\boldsymbol{w}^r[n]$ denotes the value of $\boldsymbol{w}[n]$ in the rth iteration. Since $R_u^{i,lb}[n]$ is concave with $\boldsymbol{w}[n]$, the non-convex constraint (12d) can be approximated as (18). Note that Eq. (22) shows that the solution satisfying (18) also satisfies (12d), but the reversal is not true for the most part.

In the $(r+1)$th iteration, through the approximate constraints (17) and (18), the given UAV trajectory $\boldsymbol{W}^r$ obtained in the rth iteration, the given wake-up scheduling $\boldsymbol{S}^{r+1}$, and the time slot duration $\hat{t}_{\boldsymbol{S}}^{r+1}$ obtained by solving the subproblem (13), the original subproblem (14) can be approximated as

$$\max_{\boldsymbol{W},\hat{t}}\ \hat{t} \tag{23a}$$

$$\text{s.t. } (1),(3),(12\text{e}),(17),(18). \tag{23b}$$

Since the left-hand side of the constraint (17) is convex with respect to $\boldsymbol{w}[n]$ and the right-hand side of the constraint (18) is concave with respect to $\boldsymbol{w}[n]$, it can be verified that Eq. (23) is a convex optimization problem, which can be tackled with optimization tools like CVX.

3.4 Overall algorithm

In conclusion, an algorithm is proposed to obtain the suboptimal solution to (12) by solving (13) and (23) iteratively through BCD and updating the local point at each iteration. The detailed alternating optimization is summarized as Algorithm 1.

Algorithm 1 SCA-based solutions to (12)

Input: Initialize the threshold ϵ, the trajectory $\boldsymbol{W}^0$, and the iteration index $r=0$.
1: **while** the increase of the objective value is greater than ϵ **do**
2: In the $(r+1)$th iteration, solve the linear programming problem (13) for the given $\boldsymbol{W}^r$ calculated in the rth iteration to obtain $\boldsymbol{S}^{r+1}$ and $\hat{t}_{\boldsymbol{S}}^{r+1}$;
3: Solve the convex optimization problem (23) for the given $\boldsymbol{W}^r$, $\boldsymbol{S}^{r+1}$, and $\hat{t}_{\boldsymbol{S}}^{r+1}$ to obtain $\boldsymbol{W}^{r+1}$ and $\hat{t}^{r+1}$;
4: Denote the optimal solution as $\boldsymbol{S}^*=\boldsymbol{S}^{r+1}$, $\hat{t}^*=\hat{t}^{r+1}$, and $\boldsymbol{W}^*=\boldsymbol{W}^{r+1}$;
5: Update $r=r+1$;
6: **end while**
Output: The final solutions $\boldsymbol{W}^*$, $\boldsymbol{S}^*$, and $\hat{t}^*$.

In the first step of Algorithm 1, an initial UAV trajectory $\boldsymbol{W}^0$ should be set, and we adopt a simple and systematic circular initialization as [41]. The center $\boldsymbol{C}_u$ and radius r_u of the initial trajectory $\boldsymbol{W}^0$ are determined by

$$\boldsymbol{C}_u = \sum_{i=1}^{I}\boldsymbol{L}_i/I, \tag{24}$$

$$r_u = \min\left(\frac{V_m T}{2\pi}, \frac{\|\boldsymbol{L}_i-\boldsymbol{C}_u\|}{2}\right). \tag{25}$$

For the convergence analysis of Algorithm 1, it is shown that with the given $\{\boldsymbol{W}^r,\boldsymbol{S}^r\}$ in the $(r+1)$th iteration, the solution $\{\boldsymbol{W}^r,\boldsymbol{S}^{r+1}\}$ by solving (13) is suboptimal and non-decreasing over iterations. On the other hand, for the given $\{\boldsymbol{W}^r,\boldsymbol{S}^{r+1}\}$, the solution $\{\boldsymbol{W}^{r+1},\boldsymbol{S}^{r+1}\}$ by solving the approximate

problem (23) is suboptimal and non-decreasing over iterations. Moreover, the objective value of the approximate problem (23) is a lower bound of the original subproblem (14). As a result, the objective derived from Algorithm 1 is a lower bound of the original objective (12a) and is guaranteed to converge.

Then, we analyze the complexity of Algorithm 1. Since Steps 3 and 4 of Algorithm 1 can be solved by the interior point method, the computational complexity is based on the complexity analysis of the interior-point method [42]. Step 3 involves $N-1$ linear matrix inequality (LMI) constraints of size 1, N LMI constraints of size I and $2I$ LMI constraints of size $N+1$, where $IN+1$ represents the total number of variables, and the complexity for solving Step 3 is $\sqrt{3NI+2I+N-1}(IN+1)((N-1)+NI^3+2I(N+1)^3+(IN+1)(N-1+NI^2+2I(N+1)^2)+(IN+1)^2)$, i.e., $O(I^{3.5}N^{3.5}(I+N))$. Step 4 involves 1 linear equality constraint of size 4, $N-1$ second order cone (SOC) constraints of size 5, $N-1$ SOC constraints of size 4, I SOC constraints of size $2N+1$ and I LMI constraints of size 1. The total number of variables is $2N+1$ and the complexity of solving Step 4 is $O(IN^3\sqrt{N+I})$. Therefore, the total computational complexity of Algorithm 1 is $O(I^{3.5}N^{3.5}(I+N))$.

4 Energy-efficient data collection via UAV

The time-efficient data collection scheme in Section 3 can save flight time to keep the freshness of data. Nevertheless, the limited energy of UAV is another critical challenge, and the energy efficiency should be maximized to collect more data with limited energy. Thus, we propose an energy-efficient data collection scheme via UAV in this section.

4.1 Problem formulation

The total energy consumption of the UAV includes communication-related energy and propulsion energy. We ignore communication-related energy when calculating energy efficiency because it is usually much smaller than the propulsion energy of UAVs [43,44]. The UAV propulsion power consumption depends on the UAV's speed and acceleration. We ignore the consumption caused by acceleration, which is reasonable when the acceleration time is only a small part of the total flight time [24]. For a rotary-wing UAV with the velocity V, the propulsion power consumption can be modeled as

$$P(V)=\underbrace{P_0\left(1+\frac{3V^2}{U_{\text{tip}}^2}\right)}_{\text{blade profile}}+\underbrace{P_i\left(\sqrt{1+\frac{V^4}{4v_0^4}}-\frac{V^2}{2v_0^2}\right)^{1/2}}_{\text{induced}}+\underbrace{\frac{1}{2}d_0\rho sAV^3}_{\text{parasite}}, \tag{26}$$

where U_{tip}, v_0, d_0, ρ, s, and A denote the tip speed of the rotor blade, the mean rotor induced velocity in hovering, the fuselage drag ratio, the air density, the rotor solidity, and the rotor disc area, respectively. P_0 and P_i represent the blade profile power and the induced power when $V=0$. From (26), we know that the propulsion power of a rotary-wing UAV consists of three components, i.e., the blade profile power, the induced power, and the parasite power.

As the flight cycle T is divided into N time slots, the UAV velocity in the nth time slot can be approximately given by $v[n]=\frac{\|\boldsymbol{w}[n+1]-\boldsymbol{w}[n]\|}{\delta_t}=\frac{\Delta_n}{\delta_t}$, where $\Delta_n\triangleq\|\boldsymbol{w}[n+1]-\boldsymbol{w}[n]\|$. Thus, the propulsion power consumption $P_{\text{prop}}[n]$ in the nth time slot can be written as

$$\begin{aligned}P_{\text{prop}}[n]&=P_0\left(1+\frac{3v[n]^2}{U_{\text{tip}}^2}\right)+\frac{1}{2}d_0\rho SAv[n]^3+P_i\left(\sqrt{1+\frac{v[n]^4}{4v_0^4}}-\frac{v[n]^2}{2v_0^2}\right)^{\frac{1}{2}}\\&=P_0\left(1+\frac{3\Delta_n^2}{U_{\text{tip}}^2{\delta_t}^2}\right)+\frac{1}{2}d_0\rho SA\frac{\Delta_n^3}{\delta_t^3}+P_i\left(\sqrt{1+\frac{\Delta_n^4}{4v_0^4{\delta_t}^4}}-\frac{\Delta_n^2}{2v_0^2{\delta_t}^2}\right)^{\frac{1}{2}}.\end{aligned} \tag{27}$$

Furthermore, with given $\boldsymbol{W}$ and δ_t, the UAV propulsion energy consumption E_{tot} can be written as

$$E_{\text{tot}}=\sum_{n=1}^{N}P_{\text{prop}}[n]\delta_t=P_0\sum_{n=1}^{N}\left(\delta_t+\frac{3\Delta_n^2}{U_{\text{tip}}^2\delta_t}\right)+\frac{1}{2}d_0\rho SA\sum_{n=1}^{N}\frac{\Delta_n^3}{{\delta_t}^2}+P_i\sum_{n=1}^{N}\left(\sqrt{{\delta_t}^4+\frac{\Delta_n^4}{4v_0^4}}-\frac{\Delta_n^2}{2v_0^2}\right)^{\frac{1}{2}}. \tag{28}$$

According to (8), the total amount of information $\bar{R}_{\text{tot}}$ during the period of T can be expressed as

$$\bar{R}_{\text{tot}} = \sum_{n=1}^{N} \sum_{i=1}^{I} R_u^i[n]\delta_t. \tag{29}$$

Therefore, considering (28) and (29), the energy efficiency of the UAV-aided WSN can be expressed as

$$\text{EE} = \frac{\bar{R}_{\text{tot}}}{E_{\text{tot}}} = \frac{\sum_{n=1}^{N}\sum_{i=1}^{I} R_u^i[n]\delta_t}{\sum_{n=1}^{N} P_{\text{prop}}[n]\delta_t}. \tag{30}$$

To maximize the energy efficiency by jointly optimizing the wake-up scheduling $\boldsymbol{S} = \{S_i[n], \forall i \in \mathcal{I}, \forall n\}$, the UAV trajectory $\boldsymbol{W} = \{\boldsymbol{w}[n], \forall n\}$ and the time slot duration δ_t, the optimization problem can be formulated as

$$\max_{\boldsymbol{S},\boldsymbol{W},\delta_t} \ \text{EE} \tag{31a}$$

$$\text{s.t. } (1), (2), (3), (4), (5), (9), (10). \tag{31b}$$

The problem (31) is a fractional maximization with a non-concave numerator over a non-convex denominator. In addition, the constraints (2), (9), and (10) are non-convex functions of coupled variables $\boldsymbol{S}$, $\boldsymbol{W}$, and δ_t. Thus, Eq. (31) is non-convex and difficult to solve. We use BCD and SCA to transform the non-convex problem approximately into two convex subproblems. For the fractional problem, it is solved via the Dinkelbach's method.

4.2 Subproblem 1: wake-up scheduling and time slot optimization

For any given UAV trajectory $\boldsymbol{W}$, the wake-up scheduling and time slot optimization subproblem can be formulated as

$$\max_{\boldsymbol{S},\delta_t} \ \text{EE} \tag{32a}$$

$$\text{s.t. } (2), (5), (9), (10), (12c). \tag{32b}$$

Note that $R_u^i[n]\delta_t$ is a non-convex function of coupled variables $\boldsymbol{S}$ and δ_t. Furthermore, the expression in (28) reveals that the first and second terms are convex functions with respect to δ_t, and the third term is non-convex. To make (32) more tractable, we first introduce the slack variable $a[n]$ as

$$a[n]^2 = \sqrt{{\delta_t}^4 + \frac{\Delta_n^4}{4v_0^4}} - \frac{\Delta_n^2}{2v_0^2}, \ \forall n \in \mathcal{N}, \tag{33}$$

which is equivalent to

$${\delta_t}^4 = a[n]^4 + \frac{\Delta_n^2}{v_0^2} a[n]^2, \ \forall n \in \mathcal{N}. \tag{34}$$

As a result, the third term of (28) can be replaced by $P_i \sum_{n=1}^{N} a[n]$, which is linear for $a[n]$. Thus, the total energy consumption of UAV in this subproblem is jointly convex with respect to δ_t and $a[n]$, which can be reformulated as

$$E_{\text{tot}}^A = \sum_{n=1}^{N} P_{\text{prop}}^A[n]\delta_t = P_0 \sum_{n=1}^{N} \left(\delta_t + \frac{3\Delta_n^2}{U_{\text{tip}}^2 \delta_t}\right) + \frac{1}{2} d_0 \rho S A \sum_{n=1}^{N} \frac{\Delta_n^3}{{\delta_t}^2} + P_i \sum_{n=1}^{N} a[n]. \tag{35}$$

On the other hand, we can tackle the non-convex expression $R_u^i[n]\delta_t$ by introducing the slack variable $R\_t[i]$ such that

$$R\_t[i]^2 = \sum_{n=1}^{N} R_u^i[n]\delta_t, \ \forall i \in \mathcal{I}. \tag{36}$$

After introducing two slack variables, we have

$$\text{EE} = \frac{\sum_{i=1}^{I} R\_t[i]^2}{E_{\text{tot}}^A} = \frac{\sum_{i=1}^{I} R\_t[i]^2}{\sum_{n=1}^{N} P_{\text{prop}}^A[n]\delta_t}, \tag{37}$$

and Eq. (32) can be reformulated as

$$\max_{\substack{\boldsymbol{S},\delta_t \\ a[n],R\_t[i].}} \frac{\sum_{i=1}^{I} R\_t[i]^2}{\sum_{n=1}^{N} P^A_{\text{prop}}[n]\delta_t} \tag{38a}$$

$$\text{s.t. } R\_t[i]^2 \geqslant B_i,\ \forall i \in \mathcal{I}, \tag{38b}$$

$$\sum_{n=1}^{N} (S_i[n]P_A) \leqslant E_i \frac{1}{\delta_t},\ \forall i \in \mathcal{I}, \tag{38c}$$

$$\delta_t{}^4 \leqslant a[n]^4 + \frac{\Delta_n^2}{v_0^2} a[n]^2,\ \forall n \in \mathcal{N}, \tag{38d}$$

$$R\_t[i]^2 \leqslant \sum_{n=1}^{N} R_u^i[n]\delta_t,\ \forall i \in \mathcal{I}, \tag{38e}$$

$$(2), (5), (12c). \tag{38f}$$

It can be shown that at the optimal solution to (38), the constraints (38d) and (38e) should be satisfied with equality. This is because we can always increase $R\_t[i]$ or reduce $a[n]$ to make (38d) and (38e) satisfied with equality and obtain a strictly larger objective (38a). Then, at the optimal solution to (38), the constraints (38d) and (38e) are equivalent to (34) and (36). Therefore, Eqs. (32) and (38) are equivalent.

However, Eq. (38) is non-convex due to the non-convex constraints (38b)–(38e) and the non-concavity in the numerator of the objective (38a). First, we use SCA to handle the constraints (38b)–(38d). For the constraint (38b), we introduce Proposition 2 to handle it.

Proposition 2. The non-convex constraint (38b) can be approximated as

$$R\_t_{lb}[i] \geqslant B_i,\ \forall i \in \mathcal{I}, \tag{39}$$

where

$$R\_t_{lb}[i] \triangleq R\_t^{(r)}[i]^2 + 2R\_t^{(r)}[i]\big(R\_t[i] - R\_t^{(r)}[i]\big). \tag{40}$$

Proof. In the $(r+1)$th iteration, since $R\_t[i]^2$ is a convex function with respect to $R\_t[i]$, for any given local point obtained in the rth iteration $R\_t^{(r)}[i]$, we have

$$R\_t[i]^2 \geqslant R\_t^{(r)}[i]^2 + 2R\_t^{(r)}[i]\big(R\_t[i] - R\_t^{(r)}[i]\big) \triangleq R\_t_{lb}[i]. \tag{41}$$

Obviously $R\_t_{lb}[i]$ is a linear function with respect to the slack variable $R\_t[i]$. Thus, the non-convex constraint (38b) can be approximated as (39).

Similarly, for the non-convex constraint (38c), the right-hand side is a convex function with respect to δ_t. Thus, the right-hand side can be approximated by its first-order Taylor expansions over any given local point $\delta_t{}^{(r)}$, which holds

$$\frac{1}{\delta_t} \geqslant \frac{1}{\delta_t{}^{(r)}} - \left(\frac{1}{\delta_t{}^{(r)}}\right)^2 \big(\delta_t - \delta_t{}^{(r)}\big) \triangleq \left(\frac{1}{\delta_t}\right)_{lb}. \tag{42}$$

Furthermore, for the constraint (38d), the right-hand side is a convex function with respect to $a[n]$. Thus, we have the following inequality by applying the first-order Taylor expansion at the given point $a^{(r)}[n]$.

$$a[n]^4 + \frac{\Delta_n^2}{v_0^2} a[n]^2 \geqslant a^{(r)}[n]^4 + 4a^{(r)}[n]^3\big(a[n] - a^{(r)}[n]\big) + \frac{\Delta_n^2}{v_0^2}\big(a^{(r)}[n]^2 + 2a^{(r)}[n]\big(a[n] - a^{(r)}[n]\big)\big). \tag{43}$$

For the constraint (38e), it can be reformulated as a standard SOC constraint because the hyperbolic constraint $z^2 \leqslant xy$ $(x \geqslant 0, y \geqslant 0)$ will result in $\|[2z, x-y]^\dagger\| \leqslant x + y$.

For the objective (38a), substituting the lower bound $R\_t_{lb}[i]$ for $R\_t[i]^2$ in the numerator and the objective can be reformulated as

$$\text{EE}_{lb} \triangleq \frac{\sum_{i=1}^{I} R\_t_{lb}[i]}{\sum_{n=1}^{N} P^A_{\text{prop}}[n]\delta_t} \leqslant \frac{\sum_{i=1}^{I} R\_t[i]^2}{\sum_{n=1}^{N} P^A_{\text{prop}}[n]\delta_t}, \tag{44}$$

where EE_{lb} denotes the lower bound of (38a). By replacing the non-convex constraints (38b)–(38e) with their corresponding lower bounds in (41)–(43), as well as the standard SOC constraint based on the previous discussion, we have the approximate optimization problem as

$$\max_{\substack{\boldsymbol{S},\delta_t \\ a[n],R\_t[i].}} \frac{\sum_{i=1}^{I} R\_t_{lb}[i]}{\sum_{n=1}^{N} P^{A}_{\mathrm{prop}}[n]\delta_t} \tag{45a}$$

$$\text{s.t. } R\_t_{lb}[i] \geqslant B_i,\ \forall i \in \mathcal{I}, \tag{45b}$$

$$\sum_{n=1}^{N} (S_i[n]P_A) \leqslant E_i\left(\frac{1}{\delta_t}\right)_{lb},\ \forall i \in \mathcal{I}, \tag{45c}$$

$${\delta_t}^4 \leqslant a^{(r)}[n]^4 + 4a^{(r)}[n]^3\big(a[n]-a^{(r)}[n]\big) + \frac{\Delta_n^2}{v_0^2}\big(a^{(r)}[n]^2 + 2a^{(r)}[n]\big(a[n]-a^{(r)}[n]\big)\big), \forall n \in \mathcal{N}, \tag{45d}$$

$$\left\| \left[2R\_t[i], \sum_{n=1}^{N} R_u^i[n] - \delta_t \right]^{\dagger} \right\| \leqslant \sum_{n=1}^{N} R_u^i[n] + \delta_t,\ \forall i \in \mathcal{I}, \tag{45e}$$

$$(2), (5), (12c). \tag{45f}$$

The objective (45a) is a fractional function with a concave numerator and a convex denominator, and the constraints are all convex. Therefore, we can transform (45) into an equivalent convex problem via the Dinkelbach's method and solve it with CVX.

4.3 Subproblem 2: UAV trajectory optimization

For any given wake-up scheduling $\boldsymbol{S}$ and time slot duration δ_t, the UAV trajectory can be optimized as

$$\max_{\boldsymbol{W}}\ \mathrm{EE} \tag{46a}$$

$$\text{s.t. } (1), (2), (3), (9). \tag{46b}$$

The numerator of the objective (46a) and the constraint (9) are both non-concave with respect to $\boldsymbol{w}[n]$. Note that in (18), $R_u^i[n]$ can be lower bounded by its first-order Taylor expansion $R_u^{i,lb}[n]$, which is concave with respect to $\boldsymbol{w}[n]$. Thus, the numerator of the objective (46a) and the left-hand side of the constraint (9) can be replaced by $\sum_{n=1}^{N}(R_n^{i,lb}[n]\delta_t)$.

Similar to Subsection 4.2, for the non-convex denominator $\sum_{n=1}^{N} P_{\mathrm{prop}}[n]\delta_t$, we introduce slack variables $b[n] \geqslant 0$ and have

$$b[n]^2 \leqslant \sqrt{{\delta_t}^4 + \frac{\Delta_n^4}{4v_0^4}} - \frac{\Delta_n^2}{2v_0^2}, \tag{47}$$

which is equivalent to

$$\frac{{\delta_t}^4}{b[n]^2} \geqslant b[n]^2 + \frac{\Delta_n^2}{v_0^2}. \tag{48}$$

Thus, the total energy consumption of UAV in this subproblem can be reformulated as

$$E_{\mathrm{tot}}^{B} = \sum_{n=1}^{N} P_{\mathrm{prop}}^{B}[n]\delta_t = P_0 \sum_{n=1}^{N}\left(\delta_t + \frac{3\Delta_n^2}{U_{\mathrm{tip}}^2\delta_t}\right) + \frac{1}{2}d_0\rho SA\sum_{n=1}^{N}\frac{\Delta_n^3}{{\delta_t}^2} + P_i\sum_{n=1}^{N} b[n]. \tag{49}$$

Similar to Subsection 4.2, the constraint (48) can be satisfied with equality, since we can always decrease $b[n]$ to increase the optimization goal. Although (48) is still a non-convex constraint, the right-hand side is convex with respect to $b[n]$ and $\boldsymbol{w}[n]$. By applying the first-order Taylor expansion, the lower bound can be obtained as (50).

$$\begin{aligned} b[n]^2 + \frac{\|\boldsymbol{w}[n+1]-\boldsymbol{w}[n]\|^2}{v_0^2} \geqslant & \big(b^{(r)}[n]\big)^2 + 2b^{(r)}[n]\big(b[n]-b^{(r)}[n]\big) - \frac{\|\boldsymbol{w}^{(r)}[n+1]-\boldsymbol{w}^{(r)}[n]\|^2}{v_0^2} \\ & + \frac{2}{v_0^2}\big(\boldsymbol{w}^{(r)}[n+1]-\boldsymbol{w}^{(r)}[n]\big)^{\mathrm{T}}\left(\boldsymbol{w}[n+1]-\boldsymbol{w}[n]\right). \end{aligned} \tag{50}$$

Substituting the lower bound $R_u^{i,lb}[n]$ for both the numerator of (46a) and the left-hand side of (9), and replacing the non-convex (48) with it lower bound obtained in (50), (46) can be reformulated as

$$\max_{\boldsymbol{W},b[n]} \quad \frac{\sum_{n=1}^{N}\sum_{i=1}^{I} R_u^{i,lb}[n]\delta_t}{\sum_{n=1}^{N} P_{\text{prop}}^{B}[n]\delta_t} \tag{51a}$$

$$\text{s.t.} \sum_{n=1}^{N} \left(R_n^{i,lb}[n]\delta_t\right) \geqslant B_i,\ \forall i \in \mathcal{I}, \tag{51b}$$

$$\frac{{\delta_t}^4}{b[n]^2} \leqslant \left(b^{(r)}[n]\right)^2 + 2b^{(r)}[n](b[n]-b^{(r)}[n]) - \frac{\|\boldsymbol{w}^{(r)}[n+1]-\boldsymbol{w}^{(r)}[n]\|^2}{v_0^2} + \frac{2}{v_0^2} \times \left(\boldsymbol{w}^{(r)}[n+1]-\boldsymbol{w}^{(r)}[n]\right)^{\mathrm{T}}\left(\boldsymbol{w}[n+1]-\boldsymbol{w}[n]\right),\ \forall n \in \mathcal{N}, \tag{51c}$$

$$(1), (2), (3), \tag{51d}$$

where (51a) has a concave numerator and a convex denominator with convex constraints. Hence it can be tackled with the Dinkelbach's method.

4.4 Overall algorithm

Following the similar discussion in Section 3, Algorithm 2 can be designed for the energy efficiency maximization problem (31). The optimum obtained by Algorithm 2 provides a lower bound of the objective (31a). First, since we replace the non-convex constraints with their lower bounds, the feasible region of approximate subproblems (45) and (51) are subsets of that for the original subproblems (32) and (46). Second, the approximate subproblem objectives (45a) and (51a) are both lower bounds of the original problem objective (31a).

Algorithm 2 SCA-based solutions for (31)

Input: Initialize the threshold ϵ, the trajectory $\boldsymbol{W}^0$, and the iteration index $r = 0$.
1: **while** the increase of the objective value is greater than ϵ **do**
2: In the $(r+1)$th, solve the FP problem (45) by the Dinkelbach's method for given $\boldsymbol{W}^r$ obtain in the rth iteration to obtain $\boldsymbol{S}^{r+1}$ and ${\delta_t}^{r+1}$;
3: Solve the FP problem (51) by the Dinkelbach's method for given $\boldsymbol{W}^r$, $\boldsymbol{S}^{r+1}$, and ${\delta_t}^{r+1}$ to obtain $\boldsymbol{W}^{r+1}$;
4: Denote the optimal solution as $\boldsymbol{S}^* = \boldsymbol{S}^{r+1}$, ${\delta_t}^* = {\delta_t}^{r+1}$, and $\boldsymbol{W}^* = \boldsymbol{W}^{r+1}$;
5: Update: $r = r+1$;
6: **end while**
Output: The final solutions $\boldsymbol{W}^*$, $\boldsymbol{S}^*$, and ${\delta_t}^*$.

The convergence and complexity of Algorithm 2 can be verified by similar discussion in Algorithm 1. The complexity of Steps 3 and 4 in Algorithm 2 are $O(I^{3.5}N^{3.5}(I+N))$ and $O(IN^3\sqrt{N+I})$, respectively. Thus, the overall complexity is given by $O(I^{3.5}N^{3.5}(I+N))$, which is the polynomial complexity in the worst case.

5 Simulation results

In this section, simulation results are presented to validate the two proposed schemes. Consider the scenario where a UAV serves $I = 6$ ground sensors, which are randomly distributed in a 2 km $\times$ 2 km area. The ith sensor needs to transmit $B_i = B$ bit/Hz with an energy budget of $E_i = E$ J, $i \in \mathcal{I}$, and the transmit power $P_A = 0.1$ W. The UAV propulsion power consumption parameters are specified in Table 1, and we can calculate that the optimal speed V_{me} to minimize the power consumption is 10.12 m/s. In the simulation, the UAV flies periodically at a fixed altitude $H = 100$ m with a maximum speed $V_m = 50$ m/s. The noise power is assumed to be $\sigma^2 = -110$ dBm. The channel power gain at the reference distance of 1 m is $\rho_0 = -60$ dB. Moreover, we divide the flight cycle T into $N = 60$ time slots and set the discretization factor $\gamma = 0.1$, unless otherwise specified.

Figure 2 shows the convergence of the two schemes, with $E = 10$ J and $B = 70$, 90 bit/Hz. As can be observed, the flight cycle and the energy efficiency both converge quickly. Specifically, Algorithm 1 converges within 5 iterations and Algorithm 2 converges within 30 iterations with the threshold $\epsilon = 10^{-4}$.

In order to show the superiority of the two proposed algorithms, we introduce a benchmark scheme, namely, Fly-Hover-Communicate, i.e., UAV hovers over each sensor to receive data, and flies to the

Table 1 UAV's propulsion power consumption parameters

Parameter	Value	Parameter	Value
Blade profile power in hover	$P_0 = 79.8563$ W	Induced power in hover	$P_i = 88.6079$ W
Air density	$\rho = 1.225$ kg/m^3	Rotor disc area	$A = 0.503$ m^2
Tip speed of the rotor blade	$U_{\text{tip}} = 120$ m/s	Mean rotor induced velocity in hover	$v_0 = 4.03$ m/s
Rotor solidity	$s = 0.05$	Fuselage drag ratio	$d_0 = 0.6$

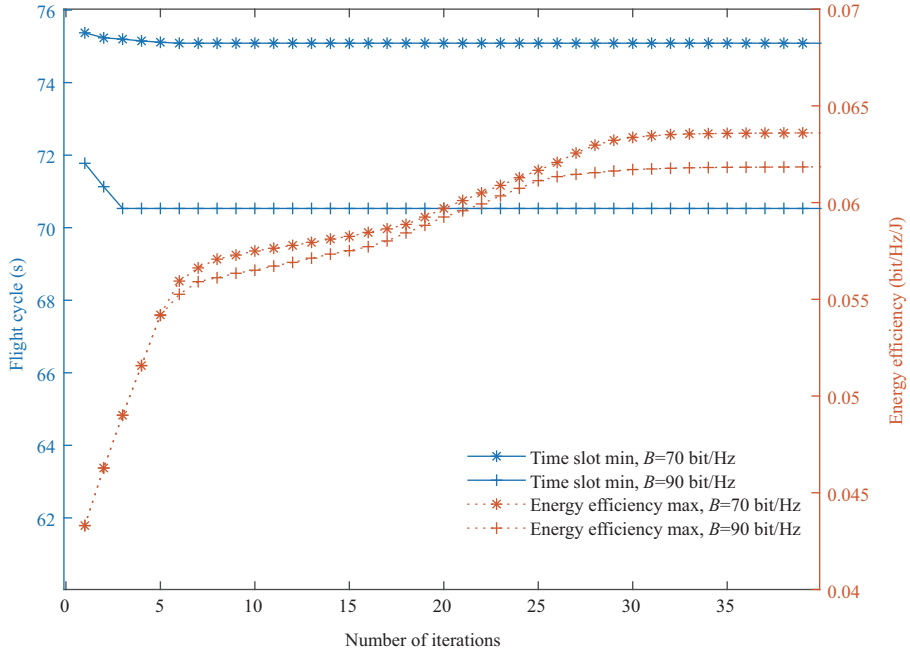

Figure 2 (Color online) Convergence of the two proposed schemes.

next sensor with the maximum speed V_m after data transmission. In Figure 3(a), we illustrate the UAV trajectories with two proposed schemes and the benchmark when $E = 10$ J. For the time slot minimization trajectory, we can observe that the UAV path is getting closer to that of the benchmark when B increases from 50 to 130 bit/Hz, although their speeds are quite different. This means that when B is sufficiently large, the UAV will spend more time visiting and flying directly to the sensors to enjoy a better channel so that more information can be uploaded to the UAV. For the energy efficiency maximization trajectory, Figure 3(a) also shows that the flight distance is shorter than that of the time slot minimization scheme when B is fixed. Furthermore, the UAV hovers around the sensors 2 and 4 for some time. This can be expected since the energy efficiency maximization speed is mostly around V_{me} to reduce the UAV propulsion power consumption while ensuring a good wireless channel, also shown in Figure 3(b).

Figure 3(b) plots the speed in the five trajectories of Figure 3(a). By combining Figures 3(a) and (b), we can find that the flight cycle of Algorithm 1 is shorter than that of Algorithm 2. For the time slot minimization scheme, the UAV almost keeps flying at the maximum speed V_m to minimize the flight cycle. For the energy efficiency maximization scheme, the UAV's speed fluctuates around V_{me} to minimize the propulsion power consumption.

In Figure 4(a), we compare the flight cycle and energy efficiency of the two proposed schemes and the benchmark with different B, where E is set to 10 J. It shows that the flight cycle of the three schemes increases as B increases from 10 to 130 bit/Hz. This is because the UAV needs longer time to transmit data to meet the growing B. Obviously, the time slot minimization scheme always outperforms the other two schemes. We also observe that the energy efficiency of the energy efficiency maximization scheme decreases while that of the other two schemes increases as B increases from 10 to 130 bit/Hz. This is due to the fundamental trade-off between the total transmission data and the propulsion power consumption. With the growth of B, T becomes larger, and both the propulsion energy consumption and the total transmission data increase. When the propulsion energy consumption increases faster, the energy efficiency decreases. Moreover, the maximal energy efficiency achieved by the energy efficiency maximization scheme is significantly higher than the other two schemes.

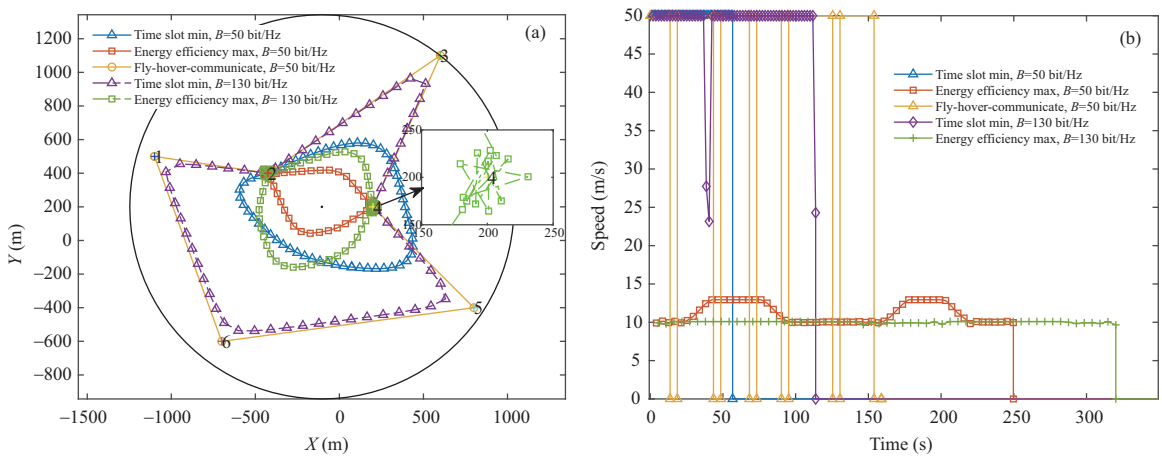

Figure 3 (Color online) (a) Optimized UAV trajectories of the two proposed schemes with the benchmark for different B; (b) UAV flying speed versus time of the two proposed schemes with the benchmark for different B.

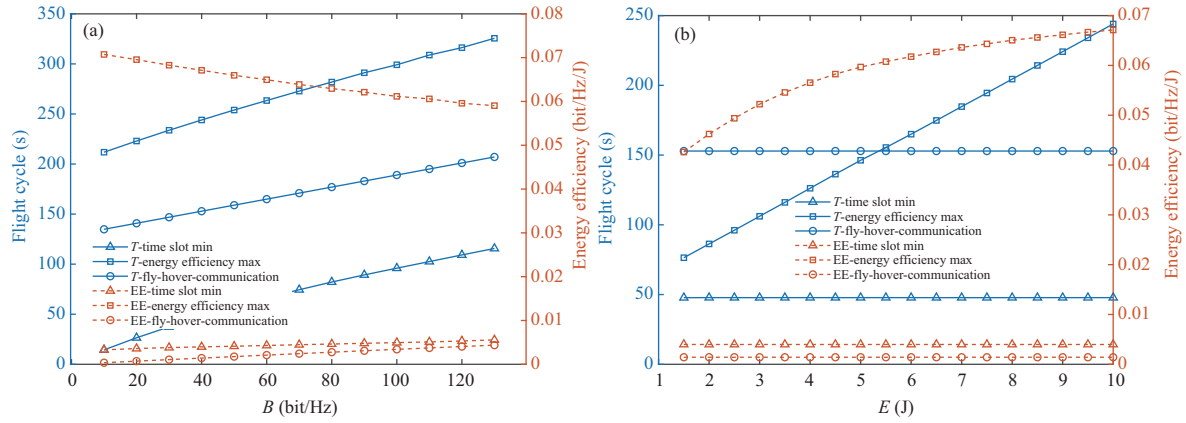

Figure 4 (Color online) (a) Flight cycle T and energy efficiency EE versus the transmission data B in the three schemes; (b) flight cycle T and energy efficiency EE versus the transmission energy E in the three schemes.

In Figure 4(b), we compare the flight cycle and the energy efficiency of the two proposed schemes and the benchmark with different E, where B is set to 40 bit/Hz. It further verifies the superiority of the two proposed schemes. One interesting note is that the flight cycle and the energy efficiency of the benchmark and the time slot minimization scheme remain constant. For the time slot minimization scheme, the reason is that when E satisfies the energy constraint (10), larger E has no effort on (10) and the optimal solution. The same is true for the benchmark. Since the speed and flight cycle of the two schemes are determined, the propulsion power consumption is constant independent of E, and the energy efficiency is also constant. On the other hand, the flight cycle and the energy efficiency of the energy efficiency maximization scheme increase as E increases. This is due to the trade-off between the transmission data and the propulsion energy consumption mentioned earlier. When E increases, it should first satisfy the data constraint (9) and the energy constraint (10), and the remaining E can be used to continue to transmit more data which will increase the flight cycle. Therefore, both the propulsion energy consumption and the total transmission data also increase. When the total transmission data increases faster, the energy efficiency becomes higher. This trade-off also leads to the different trends of energy efficiency in Figures 4(a) and (b).

Figures 5(a) and (b) illustrate the wake-up scheduling allocation of the two proposed schemes for $B = 30, 80, 130$ bit/Hz. In Figure 5(a), to minimize the flight cycle, the sensor 2 and 4 are usually allocated with fewer time slots because the UAV is closer to 2 and 4. The number of time slots becomes more balanced with the increase of B. This is because each sensor needs more time to transmit data when B increases. Figure 5(b) illustrates that the sensors 2 and 4 are allocated with more time slots, since the UAV collects data from nearby sensors like sensors 2 and 4 at speed V_{me}, the transmission rate is high and the energy consumption is low. Thus, more time slots allocated to the sensors 2 and 4 can

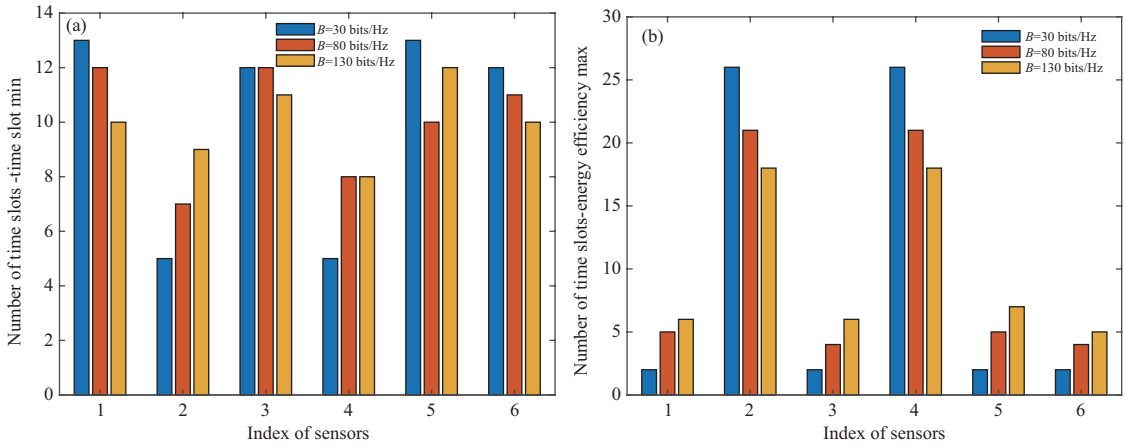

Figure 5 (Color online) Wake-up scheduling allocation for different B with (a) time-efficient data collection scheme and (b) energy-efficient data collection scheme.

improve energy efficiency.

6 Conclusion

In this paper, we study the uplink data collection in a UAV-aided WSN. By jointly optimizing the wake-up scheduling of sensors, the trajectory and the time slot, we first study the time-efficient data collection, i.e., the flight cycle minimization problem. Then, the energy efficiency is maximized for the UAV-aided WSN to collect more data with limited energy. Two algorithms based on BCD and SCA are proposed to solve the two non-convex problems respectively. Numerical results demonstrate the effectiveness of two proposed algorithms compared with the benchmark.

Acknowledgements This work was supported by National Key R&D Program of China (Grant No. 2020YFB1807002).

References

1 Zeng Y, Zhang R, Lim T J. Wireless communications with unmanned aerial vehicles: opportunities and challenges. IEEE Commun Mag, 2016, 54: 36–42
2 Gupta L, Jain R, Vaszkun G. Survey of important issues in UAV communication networks. IEEE Commun Surv Tut, 2016, 18: 1123–1152
3 Mozaffari M, Saad W, Bennis M, et al. Unmanned aerial vehicle with underlaid device-to-device communications: performance and tradeoffs. IEEE Trans Wirel Commun, 2016, 15: 3949–3963
4 Lyu J B, Zeng Y, Zhang R. Cyclical multiple access in UAV-aided communications: a throughput-delay tradeoff. IEEE Wirel Commun Lett, 2016, 5: 600–603
5 Mozaffari M, Saad W, Bennis M, et al. Efficient deployment of multiple unmanned aerial vehicles for optimal wireless coverage. IEEE Commun Lett, 2016, 20: 1647–1650
6 Al-Hourani A, Kandeepan S, Lardner S. Optimal LAP altitude for maximum coverage. IEEE Wirel Commun Lett, 2014, 3: 569–572
7 Zeng Y, Zhang R, Lim T J. Throughput maximization for UAV-enabled mobile relaying systems. IEEE Trans Commun, 2016, 64: 4983–4996
8 Cheng F, Zhang S, Li Z, et al. UAV trajectory optimization for data offloading at the edge of multiple cells. IEEE Trans Veh Technol, 2018, 67: 6732–6736
9 Pearre B, Brown T X. Model-free trajectory optimization for wireless data ferries among multiple sources. In: Proceedings of IEEE Globecom Workshops, Miami, 2010. 1793–1798
10 Lyu J B, Zeng Y, Zhang R, et al. Placement optimization of UAV-mounted mobile base stations. IEEE Commun Lett, 2017, 21: 604–607
11 Alzenad M, El-Keyi A, Lagum F, et al. 3-D placement of an unmanned aerial vehicle base station (UAV-BS) for energy-efficient maximal coverage. IEEE Wirel Commun Lett, 2017, 6: 434–437
12 Zhan C, Zeng Y, Zhang R. Energy-efficient data collection in UAV enabled wireless sensor network. IEEE Wirel Commun Lett, 2018, 7: 328–331
13 Zhan C, Zeng Y. Aerial-ground cost tradeoff for multi-UAV-enabled data collection in wireless sensor networks. IEEE Trans Commun, 2020, 68: 1937–1950
14 Xu X L, Zeng Y, Guan Y L, et al. Overcoming endurance issue: UAV-enabled communications with proactive caching. IEEE J Sel Areas Commun, 2018, 36: 1231–1244
15 Bertran E, Sànchez-Cerdà A. On the tradeoff between electrical power consumption and flight performance in fixed-wing UAV autopilots. IEEE Trans Veh Technol, 2016, 65: 8832–8840
16 Sowah R A, Acquah M A, Ofoli A R, et al. Rotational energy harvesting to prolong flight duration of quadcopters. IEEE Trans Ind Appl, 2017, 53: 4965–4972
17 Zeng Y, Xu X L, Zhang R. Trajectory design for completion time minimization in UAV-enabled multicasting. IEEE Trans Wirel Commun, 2018, 17: 2233–2246

18 Zhan C, Zeng Y. Completion time minimization for multi-UAV-enabled data collection. IEEE Trans Wirel Commun, 2019, 18: 4859–4872
19 Gong J, Chang T H, Shen C, et al. Flight time minimization of UAV for data collection over wireless sensor networks. IEEE J Sel Areas Commun, 2018, 36: 1942–1954
20 Zong J Y, Shen C, Cheng J, et al. Flight time minimization via UAV's trajectory design for ground sensor data collection. In: Proceedings of the 16th International Symposium on Wireless Communication Systems (ISWCS), Oulu, 2019. 255–259
21 Jiang X, Sheng M, Zhao N, et al. Green UAV communications for 6G: a survey. Chin J Aeronaut, 2021. doi: 10.1016/j.cja.2021.04.025
22 Bramwell A, Done G, Balmford D. Bramwell's Helicopter Dynamics. Oxford: Butterworth-Heinemann, 2001
23 Di Franco C, Buttazzo G. Energy-aware coverage path planning of UAVs. In: Proceedings of IEEE International Conference on Autonomous Robot Systems and Competitions, 2015. 111–117
24 Zeng Y, Xu J, Zhang R. Energy minimization for wireless communication with rotary-wing UAV. IEEE Trans Wirel Commun, 2019, 18: 2329–2345
25 Zhang S W, Zeng Y, Zhang R. Cellular-enabled UAV communication: a connectivity-constrained trajectory optimization perspective. IEEE Trans Commun, 2019, 67: 2580–2604
26 Yan H, Chen Y F, Yang S H. UAV-enabled wireless power transfer with base station charging and UAV power consumption. IEEE Trans Veh Technol, 2020, 69: 12883–12896
27 Li K, Ni W, Wang X, et al. Energy-efficient cooperative relaying for unmanned aerial vehicles. IEEE Trans Mobile Comput, 2016, 15: 1377–1386
28 Hua M, Wang Y, Zhang Z M, et al. Power-efficient communication in UAV-aided wireless sensor networks. IEEE Commun Lett, 2018, 22: 1264–1267
29 Zeng Y, Zhang R. Energy-efficient UAV communication with trajectory optimization. IEEE Trans Wirel Commun, 2017, 16: 3747–3760
30 Yang G, Dai R, Liang Y C. Energy-efficient UAV backscatter communication with joint trajectory design and resource optimization. IEEE Trans Wireless Commun, 2021, 20: 926–941
31 Pang X W, Tang J, Zhao N, et al. Energy-efficient design for mmWave-enabled NOMA-UAV networks. Sci China Inf Sci, 2021, 64: 140303
32 Tseng P. Convergence of a block coordinate descent method for nondifferentiable minimization. J Optim Theor Appl, 2001, 109: 475–494
33 Beck A, Ben-Tal A, Tetruashvili L. A sequential parametric convex approximation method with applications to nonconvex truss topology design problems. J Glob Optim, 2010, 47: 29–51
34 Solomon D, Pluta V. Algorithms for Generalized Fractional Programming. Cambridge: Cambridge University Press, 2000
35 Dai H B, Zhang H Y, Hua M, et al. How to deploy multiple UAVs for providing communication service in an unknown region? IEEE Wirel Commun Lett, 2019, 8: 1276–1279
36 Yang L, Meng F X, Zhang J Y, et al. On the performance of RIS-assisted dual-hop UAV communication systems. IEEE Trans Veh Technol, 2020, 69: 10385–10390
37 Yang L, Chen J C, Hasna M O, et al. Outage performance of UAV-assisted relaying systems with RF energy harvesting. IEEE Commun Lett, 2018, 22: 2471–2474
38 Lin X Q, Yajnanarayana V, Muruganathan S D, et al. The sky is not the limit: LTE for unmanned aerial vehicles. IEEE Commun Mag, 2018, 56: 204–210
39 Zhou F H, Wu Y P, Hu R Q, et al. Computation rate maximization in UAV-enabled wireless-powered mobile-edge computing systems. IEEE J Sel Areas Commun, 2018, 36: 1927–1941
40 Hua M, Yang L X, Li C G, et al. Throughput maximization for UAV-aided backscatter communication networks. IEEE Trans Commun, 2020, 68: 1254–1270
41 Wu Q Q, Zeng Y, Zhang R. Joint trajectory and communication design for multi-UAV enabled wireless networks. IEEE Trans Wirel Commun, 2018, 17: 2109–2121
42 Wang K Y, So A M C, Chang T H, et al. Outage constrained robust transmit optimization for multiuser MISO downlinks: tractable approximations by conic optimization. IEEE Trans Signal Process, 2014, 62: 5690–5705
43 Ju H, Zhang R. User cooperation in wireless powered communication networks. In: Proceedings of IEEE Global Communications Conference, Austin, 2014. 1430–1435
44 Ju H, Zhang R. Optimal resource allocation in full-duplex wireless-powered communication network. IEEE Trans Commun, 2014, 62: 3528–3540